International Journal of Bifurcation and Chaos, Vol. 5, No. 3 (1995) 779–796

A GEOMETRIC ANALYSIS OF STABILITY REGIONS FOR A LINEAR DIFFERENTIAL EQUATION WITH TWO DELAYS

JOSEPH M. MAHAFFY and KATHRYN M. JOINER
Department of Mathematical Sciences,
San Diego State University, San Diego, CA 92182-0314, USA

PAUL J. ZAK
Department of Economics,
University of Pennsylvania, Philadelphia, PA 19104-6297, USA

Received January 7, 1993; Revised July 10, 1994

We describe an algorithmic approach for determining the geometry of the region of stability for a linear differential equation with two delays. Numerous applications utilize two-delay differential equations and require a framework to assay stability. The imaginary and zero solutions of the characteristic equation, where bifurcations in stability occur, produce an infinite set of surfaces in the coefficient parameter space. A methodology is outlined for identifying which of these surfaces form the boundary of the stability region. For a range of delays, the stability region changes in only three ways, starting at an identified initial point and becoming more complex as one coefficient increases. Detailed graphical analyses, including three-dimensional plots, show the evolution of the stability surface for given ratios of delays, highlighting variations across delays. The results demonstrate that small changes in the delay ratio cause significant changes in the size and shape of the stability region.

1. Introduction

Models using delay differential equations have appeared with increasing frequency in a variety of applications. Time delays are introduced into mathematical models to account for systems containing differing processes, such as staggered rates of production. Dynamic models with discrete lags have spanned the scientific literature, from biology to optics. Often there are multiple stages to the model that require several time delays, such as insects passing through a series of instar stages. The population of a single species, which is affected by both regeneration and reproduction time lags, has been modeled with two constant delays [Braddock & van den Driessche, 1981, 1983]. Models of interspecies competition or parasitoid–host systems use multiple delays to account for maturation times [MacDonald, 1986, 1989; Murdoch *et al.*, 1987]. Epidemic models require incubation times, which can be modeled with two discrete delays [Cooke & Yorke, 1973; MacDonald, 1989]. Two delays enter physiological models of development and disease such as erythropoiesis [Bélair *et al.*, 1994], cyclic granulopoiesis [MacDonald, 1980], and cyclical neutropenia [MacDonald, 1979]. Neurological diseases have been studied with two delay models [Beuter *et al.*, 1993]. In physical systems, multiple time delays in control loops result in complicated dynamical behavior as seen in certain optics problems [Marriott *et al.*, 1989; Mizuno & Ikeda, 1989] or robotic control

problems [Haller & Stépán, 1991]. In economics, the optimal production decision for an oligopoly with information lags has been modeled using multiple delays [Howroyd & Russell, 1984].

Many deterministic models that include two time delays produce complicated dynamics. One etiology for this behavior occurs when parameter values in the linearized system have two purely imaginary pairs of eigenvalues. This scenario is similar to that for the planar Hopf bifurcation, but causes the bifurcation dynamics to occur on a two-torus. Guckenheimer and Holmes [1983] (in Chap. 7.5) illustrate the variety of bifurcations which can occur on a two-torus and state that chaotic dynamics can occur in nonlinear problems. Bifurcation analysis examining the two-torus for two-delay problems with some applications can be found in Bélair & Campbell [1994], Beuter *et al.* [1993], and Campbell & Bélair [1993]. Part of the geometric approach in this paper traces the intersections of two pairs of purely imaginary eigenvalues (or a zero root of the characteristic equation and an imaginary pair of eigenvalues) in a linear two-delay differential equation.

Mathematical analyses of multiple-delay differential equations are often restricted to special cases due to the inherent high dimensionality of the problems. Several studies have analyzed the region of asymptotic stability for linear delay differential equations with multiple delays, where the delays vary over a range of values [Boese, 1993; Cooke & Ferreira, 1983; Hale *et al.*, 1985; Silkowski, 1979]. These results establish the necessary and sufficient conditions for the largest cone-shaped regions of stability independent of the delays. Lyapunov functionals are used to find regions of uniform asymptotic stability for a general multiple delay problem [Busenberg & Cooke, 1984]. However, when the delays are fixed, the region of stability no longer retains a convex shape [Bélair, 1987; Hale, 1979; Stépán, 1987]. As one parameter varies, a multiple-delay differential equation can go through a series of stability switches [Cooke & van den Driessche, 1986].

This paper considers a scalar linear first order differential equation with two delays. The general form of this equation is

$$\dot{y}(t) + ay(t) + by(t - r_1) + cy(t - r_2) = 0\,. \quad (1.1)$$

The stability of (1.1) depends on its five parameters and can be determined by locating the complex roots of the associated characteristic equation:

$$\lambda + a + be^{-r_1\lambda} + ce^{-r_2\lambda} = 0\,. \quad (1.2)$$

The zero solution of (1.1) is asymptotically stable if all roots of (1.2) have negative real parts. Since this characteristic equation is an exponential polynomial with two different exponential functions in the eigenvalues λ, the analysis is particularly difficult.

Techniques that locate the roots of (1.2) have been investigated in a number of special cases. The one-delay problem ($c = 0$) has been completely solved by Hayes [1950]. The case $a = 0$ and $r_1 = 1$ with other specific restrictions has been analyzed [Nussbaum, 1975; Ruiz-Claeyssen, 1976]. After normalizing one of the parameters, the several authors characterize the stability region of the four parameter problem using two-dimensional projections in the parameter space. A number of papers [Bélair & Campbell, 1994; Braddock & van den Driessche, 1981; Hale, 1979] have performed a more complete analysis of (1.1) for the case $a = 0$, which is important in applications. When $a \neq 0$, the problem becomes more difficult to characterize. Bélair [1987] and Zaron [1987] study the stability region in the bc-parameter space, while Hale and Huang [1993] give a geometrical description of the stability for (1.1) in the r_1r_2-parameter space.

This paper examines the stability of (1.1) after one of the delays has been normalized by a rescaling of time ($\tau = t/r_1$). Without loss of generality, one can assume that $r_1 > r_2$, so if $A = r_1a$, $B = r_1b$, $C = r_1c$, and $R = r_2/r_1$, then (1.1) reduces to the four parameter problem:

$$\dot{y}(\tau) + Ay(\tau) + By(\tau - 1) + Cy(\tau - R) = 0\,, \quad 0 < R < 1\,. \quad (1.3)$$

The analysis considers a range of values for the delay R, and systematically constructs the complete stability surface in the coefficient parameter space as the coefficient A of the undelayed term in (1.3) is increased. The solutions of the characteristic equation for (1.3) with purely imaginary or zero roots form an infinite set of surfaces in the coefficient parameter space. The boundary of the stability region is a surface created from intersecting portions of this infinite set of surfaces. At this boundary either Hopf bifurcations at various frequencies occur or there is a zero root crossing. Section 2 provides the basic definitions and theorems that are used to describe the evolution of the stability surface and

applies them to the case $R = \frac{1}{3}$. For a given delay, the stability surface comes to a point at some minimum value of A, then as A increases the stability surface becomes more complex as higher frequency Hopf bifurcations affect the boundary of the stability region. However, there are only three ways that new bifurcation surfaces enter the boundary of the stability region, yielding discernable patterns in its construction. Three-dimensional graphics illustrate the complete stability surfaces for several values of R.

Sections 3 and 4 use the techniques developed in Sec. 2 to show how the stability surfaces change as the delay R varies. This problem is quite complicated as small changes in the delay often elicit significant variations in the size and shape of the stability region. Still our methodology shows that for bounded values of R and A, there are only a finite number of bifurcation surfaces that are needed to construct the boundary of the stability region. Local continuity with respect to the parameters allows us to track the evolution of this boundary in ABC parameter space.

2. An Example — Tools and Techniques for Analysis of the Two-Delay Problem

In this section a set of definitions and theorems are developed to characterize the stability region for (1.3). The case $R = \frac{1}{3}$ is used to illustrate these principles and demonstrate the complexity of the three-dimensional stability region. Later sections show how the stability surface evolves as R varies, yet most of the significant features of two-delay differential equation stability surfaces are apparent when $R = \frac{1}{3}$.

The two-delay differential equation given by (1.3) is an infinite-dimensional problem. To find a solution for $\tau > 0$ initial data must be given over an interval of time reflecting the past history. If $\phi(\tau)$ is a continuous function defined for $\tau \in [-1, 0]$ and $y(\tau) = \phi(\tau)$, then there exists a unique, continuously differentiable solution $y(\tau)$ to (1.3) for all $\tau > 0$ [Hale, 1977]. The trivial solution, $y(\tau) \equiv 0$, is the unique equilibrium solution of (1.3), provided $A+B+C \neq 0$. Stability of the equilibrium solution can be determined using the characteristic equation associated with (1.3),

$$\lambda + A + Be^{-\lambda} + Ce^{-\lambda R} = 0\,, \qquad (2.1)$$

which contains four parameters. This study examines the stability region in the three-dimensional space of the parameters A, B, and C for fixed values of R. The analytical approach we take in locating the stability region parallels Bélair [1987] and Zaron [1987], who use the D-decomposition partitions of El'sgol'ts [1966].

Graphical analysis shows that the stability region is a connected set in the ABC-parameter space for $R \in (0, \frac{1}{2}]$, though some BC-cross-sections have disjoint regions of stability as has been noted by other authors [Bélair, 1987; Bélair & Campbell, 1994; Hale & Huang, 1993; Stépán, 1987]. Our work suggests that the three-dimensional stability region is connected for all $0 < R < 1$. It is clear from (2.1) that the positive half-line $A > 0$ must lie within the stability region. A complete analysis of the stability region has been performed for the one-delay case (either $B = 0$ or $C = 0$) [Hayes, 1950] and our results for (1.3) are consistent with these. For the nondegenerate case, B and $C \neq 0$ we examine the stability properties of (1.3) extended to the entire ABC-parameter space. A partial answer is provided by the following theorem:

Theorem 2.1 (Minimum Region of Stability). *For $A > |B|+|C|$, all solutions λ to (2.1) have $\mathrm{Re}\,\lambda < 0$. Thus, the differential equation (1.3) is asymptotically stable inside the pyramidal-shaped region centered about the positive A-axis independent of R.*

The proof of this theorem can be found in Boese [1993] and Zaron [1987].

The above result provides a *Minimum Region of Stability* (MRS). However, questions remain regarding how much larger the region of stability is for (1.3), and how this region varies with R. The search for the boundary of the region focuses on the image of the imaginary axis in the λ-plane. When $\lambda = 0$, any point on the plane $A+B+C = 0$ satisfies (2.1). This plane separates the ABC-parameter space into two parts where the region with $A+B+C < 0$ is unstable as it contains at least one real positive root. Since the plane $A + B + C = 0$ bounds one face of the MRS given in Theorem 2.1, one part of the stability region is comprised of this real root crossing surface. The remaining surfaces bounding the stability region are found by examining the imaginary roots, $\lambda = i\omega$, where Hopf bifurcations occur.

The next step of the analysis is to determine the image of the imaginary axis in the ABC-parameter

space. If $\lambda = i\omega$, then (2.1) can be written

$$A + B\cos(\omega) + C\cos(\omega R) + i(\omega - B\sin(\omega) - C\sin(\omega R)) = 0. \quad (2.2)$$

By splitting this into its real and imaginary parts and solving for B and C, we obtain the following parametric equations:

$$B(\omega) = \frac{A\sin(\omega R) + \omega\cos(\omega R)}{\sin(\omega(1-R))}, \qquad C(\omega) = -\frac{A\sin(\omega) + \omega\cos(\omega)}{\sin(\omega(1-R))}. \quad (2.3)$$

These equations are defined on the intervals $\frac{(j-1)\pi}{1-R} < \omega < \frac{j\pi}{1-R}$, j being an integer. As A varies with $\omega \in \left(\frac{(j-1)\pi}{1-R}, \frac{j\pi}{1-R}\right)$, Eqs. (2.3) generate a surface in the ABC-parameter space. For fixed A, (2.3) produces cross-sectional curves where the eigenvalues of (2.1) cross the imaginary axis in the BC-plane. A definition clarifies the range of frequencies at which bifurcations occur.

Definition. The jth bifurcation surface (curve) is the surface (curve) generated by the parametric equations (2.3) with $\frac{(j-1)\pi}{1-R} < \omega < \frac{j\pi}{1-R}$, where j is a positive integer.

Hayes [1950] showed that the stability region for the one delay problem ($C = 0$) is completely determined by the first bifurcation curve and the line $A = -B$. For the two delay problem (1.3), the first bifurcation surface and the plane $A + B + C = 0$ do not give the complete stability picture. However, the first bifurcation surface can be used to bound the stability region and provides valuable information on how to begin the study of the stability surface for $R \leq \frac{1}{2}$.

The first bifurcation surface intersects the $A + B + C = 0$ plane as $\omega \to 0$. From (2.3), this occurs when $B = (AR + 1)/(1 - R)$ and $C = -(A + 1)/(1 - R)$, which is the line

$$\frac{A+1}{1-R} = \frac{B-1}{R} = -C \quad (2.4)$$

in the ABC-parameter space. For a range of A values with ω increasing from zero, the first bifurcation surface intersects the $A + B + C = 0$ plane a second time forming a curve in BC-space. As A decreases this curve intersects the line (2.4) at A_0, and the initial point from which the stability surface emanates is determined.

For most values of $R \in (0, \frac{1}{2}]$, A_0 is the smallest value of A for which (1.3) is stable. A complication arises from the manner by which the second bifurcation surface adjoins this stability surface. When $R < R_0$ where $R_0 \simeq 0.0117$, the smallest value of A for which (1.3) is stable is less than A_0 due to a self-intersecting bifurcation surface, which is discussed below.

The following theorem summarizes how we begin our stability study for (1.3):

Theorem 2.2. *If $R > R_0$ and $A < -(R + 1)/R$, then (1.3) is unstable independent of B and C. Geometrically, the stability surface comes to a point at*

$$(A_0, B_0, C_0) = \left(-\frac{R+1}{R}, \frac{R}{R-1}, \frac{1}{R(1-R)}\right), \quad (2.5)$$

and for some range of $A > A_0$, the stability region is bounded by the first bifurcation surface and the $A + B + C = 0$ plane.

The proof of this theorem is found in Mahaffy *et al.* [1993].

For each fixed $R > R_0$, we begin our studies with $A = A_0$. Subsequently, the evolution of the stability region is followed as A increases. Figure 2.1 presents the three-dimensional stability surface for the case $R = \frac{1}{3}$. The initial point from Theorem 2.2 is clearly visible and occurs at

$$(A_0, B_0, C_0) = \left(-4, -\frac{1}{2}, \frac{9}{2}\right).$$

The surface is created by fixing the values of A and determining the stability region in the BC-cross-sectional plane. Theorem 2.2 states that initially the stability region is enclosed by part of the first bifurcation surface (blue) and a section of the $A + B + C = 0$ plane (violet). As A increases with $R \leq \frac{1}{2}$, there are three modes by which higher frequency bifurcation surfaces encroach upon the boundary of the stability region. Each of these modalities can be seen in Fig. 2.1 and is defined below. Figure 2.1 shows parts of the second, fourth, and sixth bifurcation surfaces in green, red, and orange, respectively, are also part of the boundary of the stability region. Details on how these surfaces enter the stability diagram follow.

For most values of A, the curves in the BC-plane generated by (2.3) tend to infinity parallel to the lines $B + C = 0$ or $B - C = 0$ as $\omega \to \frac{j\pi}{1-R}$. However, for certain values of A, the equations given by (2.3) become indeterminate at $\frac{j\pi}{1-R}$. Define these *transition* values of A by A_j^*, where

$$A_j^* = -\frac{j\pi}{1-R} \cdot \cot\left(\frac{jR\pi}{1-R}\right), \quad j = 1, 2, \ldots \quad (2.6)$$

At a transition the jth and $(j+1)$st bifurcation curves coincide at the point (B_j^*, C_j^*), where

$$B_j^* = (-1)^j \frac{(1-R)\cos\left(\frac{jR\pi}{1-R}\right) - jR\pi \csc\left(\frac{jR\pi}{1-R}\right)}{(1-R)^2}, \quad (2.7)$$

$$C_j^* = -(-1)^j \frac{(1-R)\cos\left(\frac{j\pi}{1-R}\right) - j\pi \csc\left(\frac{j\pi}{1-R}\right)}{(1-R)^2}.$$

Along the line

$$(B - B_j^*) + (-1)^j (C - C_j^*) = 0, \quad A = A_j^*, \quad (2.8)$$

there are two roots of (2.1) on the imaginary axis with $\lambda = \pm \frac{j\pi}{1-R} i$. If the jth bifurcation surface is on the boundary of the stability region for A slightly less than A_j^*, then at $A = A_j^*$, Eq. (2.8) becomes part of the stability region's boundary, and subsequently, the $(j+1)$st bifurcation surface enters the boundary of the stability region. Our studies show that the largest local distortions in the stability surface occur near transitions.

For $R = \frac{1}{3}$, all transitions occur at $A = 0$, as Eq. (2.6) reduces to $A_j^* = 0$ whenever j is odd. When j is even, A_j^* is infinity. The only transition directly affecting the boundary of the stability region is A_1^*, which is shown in Fig. 2.1 at the stage where the green surface (second bifurcation surface) first enters the stability diagram.

The $(j+1)$st bifurcation surface, which enters the boundary of the stability region immediately after A_j^*, self-intersects for a range of A values prior to the transition. The small region enclosed by the self-intersection contains no eigenvalues of (2.1) with positive real parts; hence, (1.3) is stable within this region. Proof of the existence of this stability region can be found in Mahaffy *et al.* [1993]. Following A backwards from A_j^*, we define A_j^p as the value where the area enclosed by the self-intersection goes to zero. For $A \in (A_j^p, A_j^*)$, there is a protrusion in the stability region or a *stable spur*, which joins the region of stability of Theorem 2.2 at A_j^*. In BC-cross sections the stable spur appears to be disconnected from the principal region of stability. The three-dimensional structure maintains

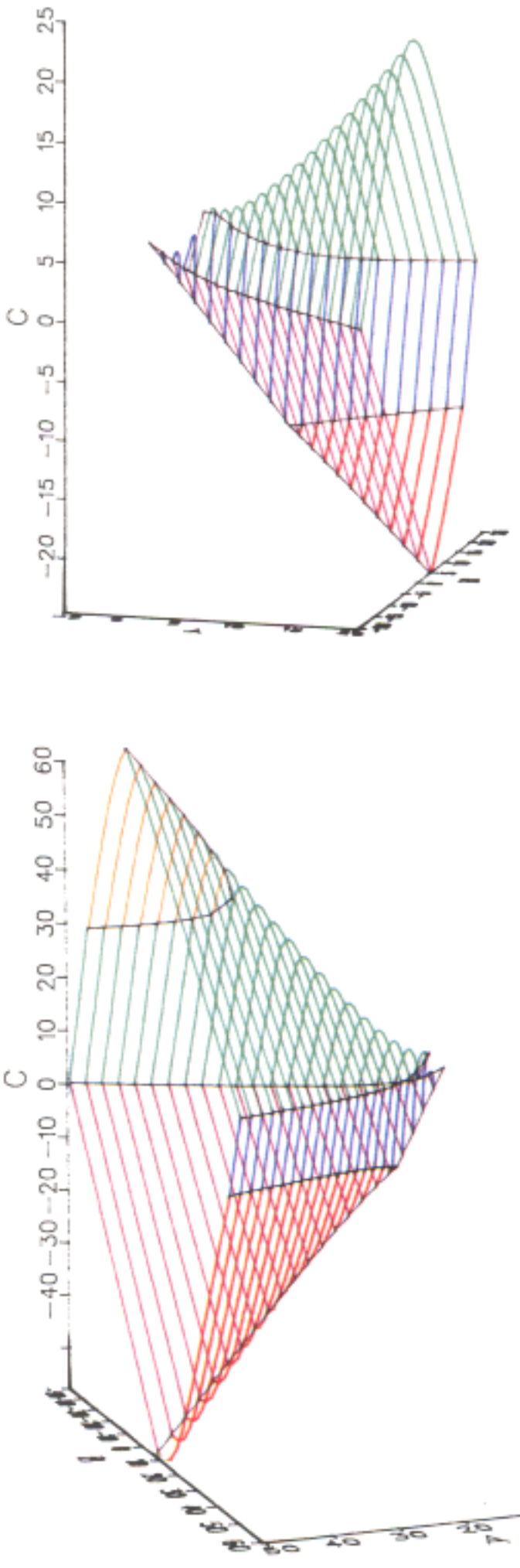

Fig. 2.1. The stability surface for the case $R = \frac{1}{3}$. The top picture shows the three-dimensional surface for $A \leq 20$, while the bottom picture shows a different angle and $A \leq 50$.

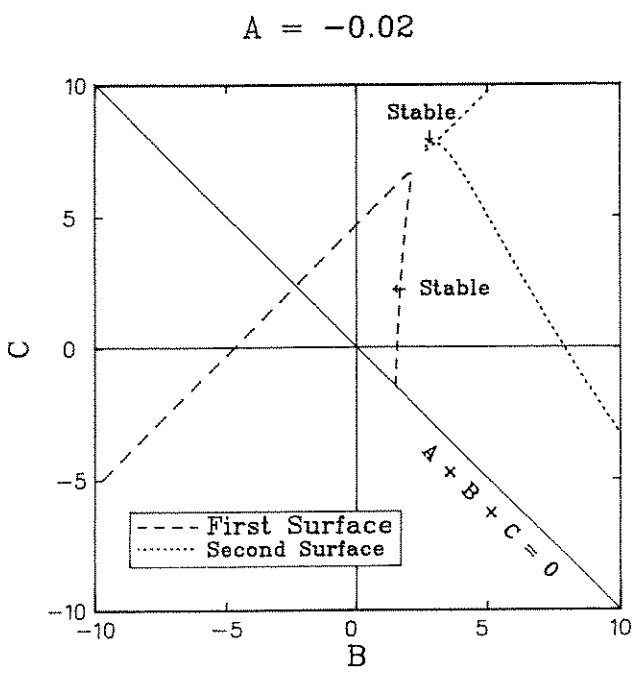

Fig. 2.2. For $R = \frac{1}{3}$ and $A = -0.02$, the stability region is bounded by the first bifurcation curve and the line $A + B + C = 0$. A stable spur appears as the second bifurcation curve self-intersects.

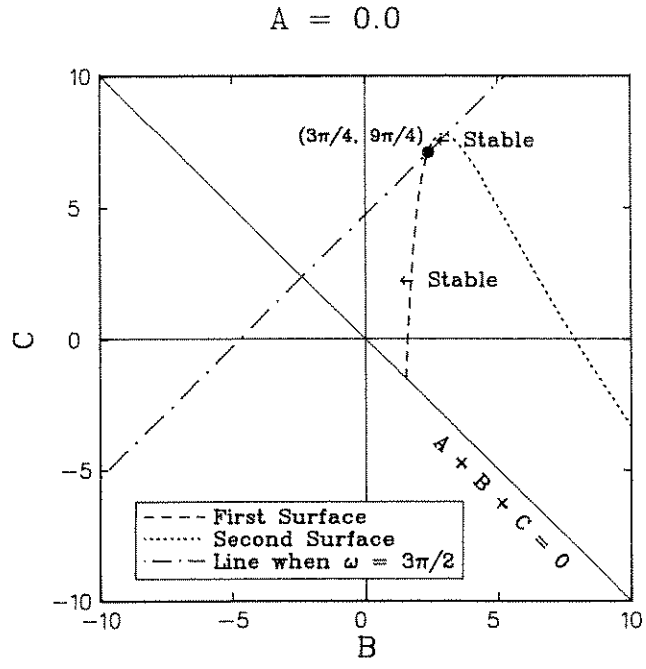

Fig. 2.3. For $R = \frac{1}{3}$ and $A_1^* = 0$, a transition occurs. The stability region of Theorem 3.2 is bounded by the first bifurcation curve and the lines $B + C = 0$ and $C - B = \frac{3\pi}{2}$. The stable spur is bounded by the second bifurcation curve and the line $C - B = \frac{3\pi}{2}$ and joins the first region of stability at the point (B_1^*, C_1^*).

connectivity between the principal region of stability and the stable spur at the transitional value A_j^*.

Details illustrating the effects of a transition with its associated stable spur on the region of stability are shown in Figs. 2.2–2.5 for the delay $R = \frac{1}{3}$. As A approaches the transitional value $A_1^* = 0$, the region of stability expands as the first bifurcation curve is stretched along the line $C - B = \frac{3\pi}{2}$ toward the second bifurcation curve. Similarly, the second bifurcation curve is drawn toward the first bifurcation curve for A near A_1^*, causing the second bifurcation curve to self-intersect as seen in Fig. 2.2. This self-intersection only exists for $A \in (A_1^p, A_1^*) \simeq (-0.117, 0)$, and encloses another region of stability. This region of stability is too small to appear in Fig. 2.1, but the distortion is clear from the transition line in black that parallels the level curves in the top figure (just prior to the second bifurcation surface shown in green). The stable spur isolates this portion of the stability region as the second bifurcation curve self-intersects, creating a loop whose area increases as A approaches A_1^*.

At the transition, $A_1^* = 0$, the first and second bifurcation curves meet at the point $(B_1^*, C_1^*) = (3\pi/4, 9\pi/4)$ as seen in Fig. 2.3. Along the line $C - B = \frac{3\pi}{2}$, which is derived from (2.8), the purely imaginary solutions $\lambda = \pm i\frac{3\pi}{2}$ satisfy (2.1). The region of stability from Theorem 2.2 is bounded by parts of the first bifurcation surface, the $A+B+C = 0$ plane, and the line $C - B = \frac{3\pi}{2}$. The stable spur is bounded by the second bifurcation surface and the line $C - B = \frac{3\pi}{2}$. The regions of stability from Theorem 2.2 and the stable spur join at the point (B_1^*, C_1^*). Subsequently, the ends of the first and second bifurcation curves swap positions near $\omega = \frac{3\pi}{2}$. Figure 2.4 shows how the first and second bifurcation curves comprise the boundary of the stability region for A slightly larger than A_1^*. For a range of $A > A_1^* = 0$, the stability region is bounded by sections of the first bifurcation surface (blue), the second bifurcation surface (green), and the $A + B + C = 0$ plane. A magnified three-dimensional picture of the transition A_1^* and its associated stable spur is shown in Fig. 2.5.

Theorem 2.1 demonstrates that for each A one corner of the MRS is given by $(B, C) = (0, -A)$. Equation (2.4) shows that the first bifurcation surface intersects the $A+B+C = 0$ plane at $(B, C) = ((AR + 1)/(1 - R), -(A + 1)/(1 - R))$, which diverges from $(0, -A)$ as A increases. Thus, a large

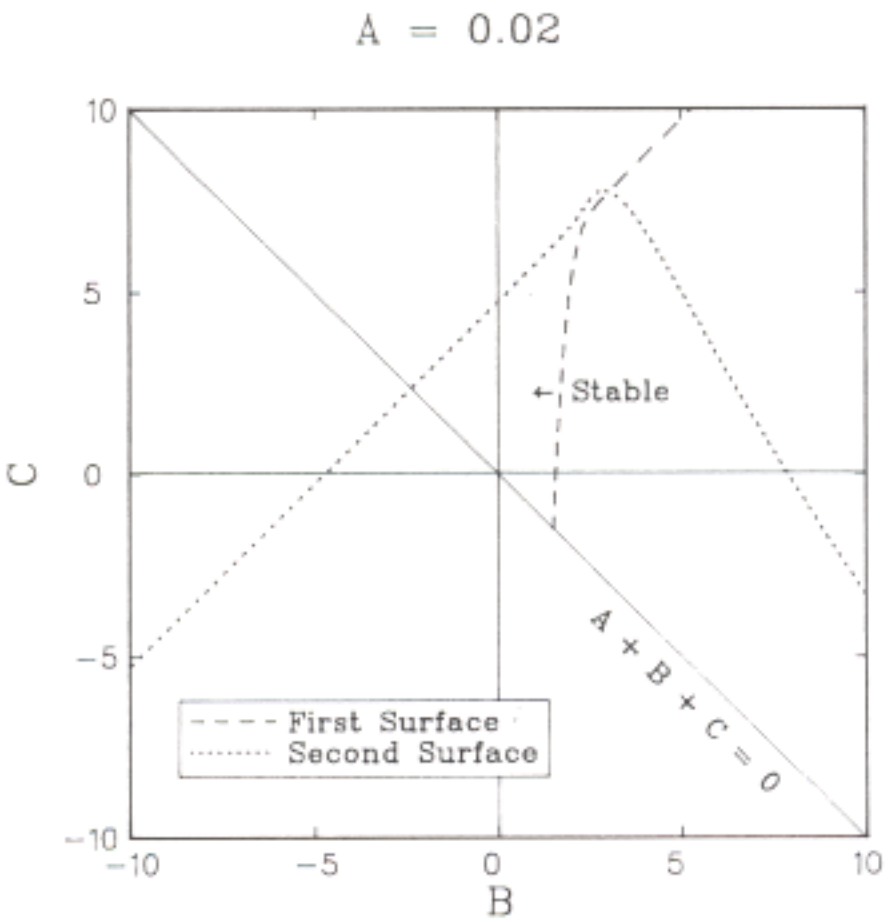

Fig. 2.4. For $R = \frac{1}{3}$ and $A = 0.02$, the stability region is bounded by the first and second bifurcation curves and the line $A + B + C = 0$.

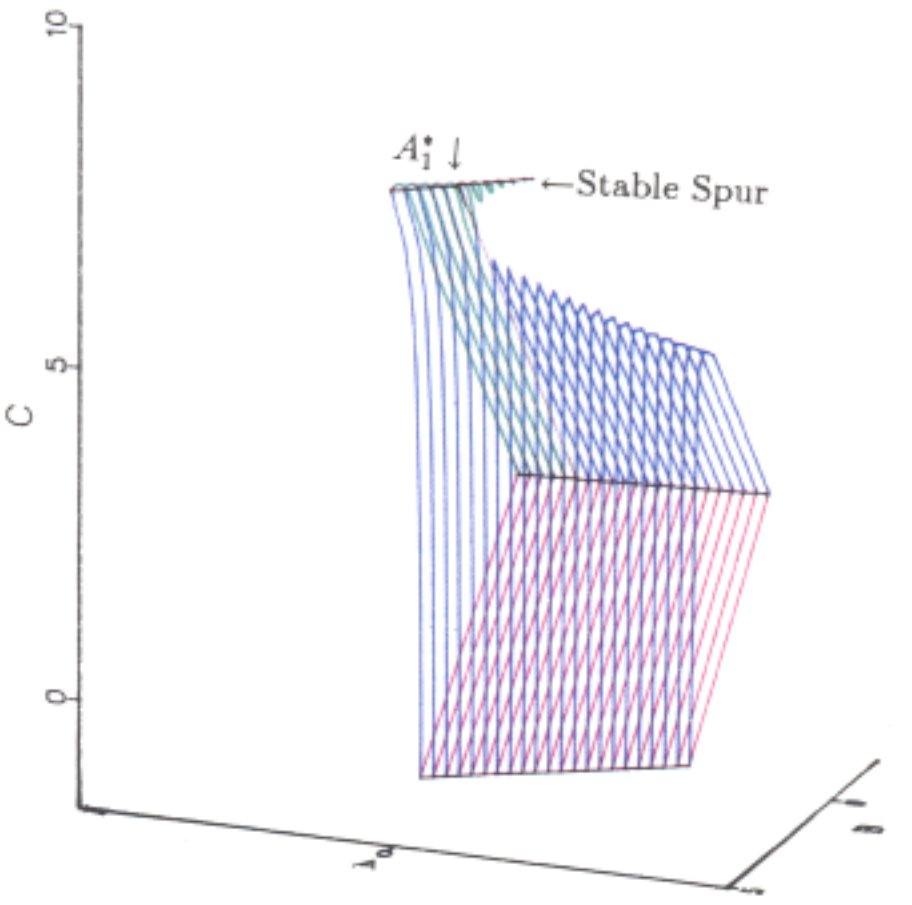

Fig. 2.5. The stability surface for $R = \frac{1}{3}$ with $A \in [-0.3, 0.1]$. This figure magnifies the region which contains the transition, A_1^*, and its associated stable spur.

gap develops between the first bifurcation surface and the lower corner of the MRS where another bifurcation surface may join the boundary of the stability region. We define the *transferral* value of $A = A_{i,j}^z$ to be the value of A where the jth bifurcation surface intersects the ith bifurcation surface at the $A+B+C=0$ plane with the jth bifurcation surface entering the boundary of the stability region for $A > A_{i,j}^z$. This is a second way in which bifurcation surfaces enter the boundary of the stability region. Often there is only one transferral value, but for some values of R a distortion of the bifurcation surface near the $A + B + C = 0$ plane caused by a transition results in several transferrals.

When $R = \frac{1}{3}$ there is a transferral $A_{1,4}^z$, where the first bifurcation surface, the fourth bifurcation surface (red), and the $A + B + C = 0$ plane intersect at the point $(A, B, C) \simeq (7.1, 5.0, -12.1)$. Subsequently, the fourth bifurcation surface enters the boundary of the stability region, and for a range of $A > A_{1,4}^z$, the stability region is bounded by sections of the first, second, and fourth bifurcation surfaces and the $A + B + C = 0$ plane. These are the only surfaces needed for the top stability surface in Fig. 2.1.

The third route through which bifurcation surfaces enter the boundary of the stability region is a tangency. We define the *tangential* value of $A = A_{i,j}^t$, to be the value of A at which the jth bifurcation curve becomes tangent to the ith bifurcation curve that is already part of the stability boundary. As A increases from $A_{i,j}^t$, the new bifurcation curve is incorporated into the boundary of the stability region, separating segments of the bifurcation curve to which it was tangent.

When $R = \frac{1}{3}$, the sixth bifurcation curve (orange) becomes tangent to the second bifurcation curve near $(A, B, C) = (30.7, -12.0, 33.8)$. Subsequently, the sixth bifurcation surface enters the boundary of the region of stability for $A > A_{2,6}^t \simeq 30.7$. The next change in the stability surface occurs at $A = A_{4,8}^t \simeq 50.4$ where the eighth bifurcation surface becomes tangent to the fourth bifurcation surface. This point of tangency is near $(A, B, C) = (50.4, 18.7, -54.1)$. As A increases further, additional tangencies occur, injecting more of the even bifurcation surfaces into the boundary of the stability region.

For a fixed $R < \frac{1}{2}$, we determine the boundary of the stability region in the BC-plane by examining changes that occur as A increases. From the initial point given in Theorem 2.2, additional bifurcation curves enter the boundary of the stability region by one of the methods listed above,

i.e., a transition (which includes an associated stable spur), a transferral, or a tangency. The complete three-dimensional bifurcation stability surface is generated by combining these cross-sectional graphs. For any fixed value of A, there are a finite number of the bifurcation surfaces that generate the boundary of the stability region. Thus, by combining BC cross-sections we can completely characterize the region of stability in ABC-parameter space for any delay $R \leq \frac{1}{2}$.

3. The Stability Region for R near $\frac{1}{3}$

The key to developing the three-dimensional stability region is determining the junctures where changes in the stability surface occur. When two bifurcation surfaces meet on the stability surface, they share the same (A, B, C) value and two pairs of purely imaginary eigenvalues $\lambda = i\omega$, each satisfying (2.3) for a given A. As noted in the introduction, if (1.3) is the linearization of a nonlinear problem, then these junctures could lead to complicated dynamics [Campbell & Bélair, 1993; Guckenheimer & Holmes, 1983]. Numerically, the two pairs of eigenvalues are found by Newton's method and are followed in 3-dimensions by slowly increasing A. Once the ω values are found for the ends of a bifurcation curve in the BC-cross-sections, Eq. (2.3) are used to generate this segment along the boundary of the stability region. The most difficult aspect of constructing the three-dimensional stability surface is determining which bifurcation surfaces comprise the boundary of the stability region and the values of A at which they enter.

This section examines local changes in the stability region as R increases or decreases from $\frac{1}{3}$. For a certain range of A values and small variations in R, the structure of the stability region closely resembles the case $R = \frac{1}{3}$ shown in the previous section. However, there are some significant differences for particular values of R near $\frac{1}{3}$. Our discussion in this section illustrates the complexity of the stability surface by focusing on delays in the interval $R \in [0.31, 0.35]$. It shows how to construct the stability surface in ABC parameter space by tracking the transitions, transferrals, and tangencies.

Figure 3.1 provides an overview of changes in the stability region boundary as a function of A, listing the type of change in each case. The figure shows that there is little change in the initial point (A_0, B_0, C_0) on the boundary of the stability region for $R \in [0.31, 0.35]$. On this interval the first change in the stability surface is the transition A_1^*, which also exhibits little variation over the given delays. Prior to A_1^*, the second bifurcation surface self-intersects creating a stable spur on the interval (A_1^p, A_1^*), which joins the stability surface emanating from A_0 at A_1^*. The length of the interval (A_1^p, A_1^*) decreases from 0.159 for $R = 0.31$ to 0.092 for $R = 0.35$, indicating that the stable spur is a minor part of the stability surface. Consequently, Figs. 2.2–2.5 are representative of the geometry of the stability surfaces near A_1^* for $R \in [0.31, 0.35]$.

As A increases, Fig. 3.1 shows that for most values of $R \in [0.31, 0.35]$ the next change in the stability surface is the tranferral $A_{1,4}^z$, as is the case when $R = \frac{1}{3}$. However, near $R \simeq 0.311$ this transferral no longer occurs due to another transition, A_4^*. As R decreases from $\frac{1}{3}$, the value A_4^* decreases with the transition occurring along the line given by (2.8), which can be shown to lie below the $A + B + C = 0$ plane. This decrease in A_4^* causes the

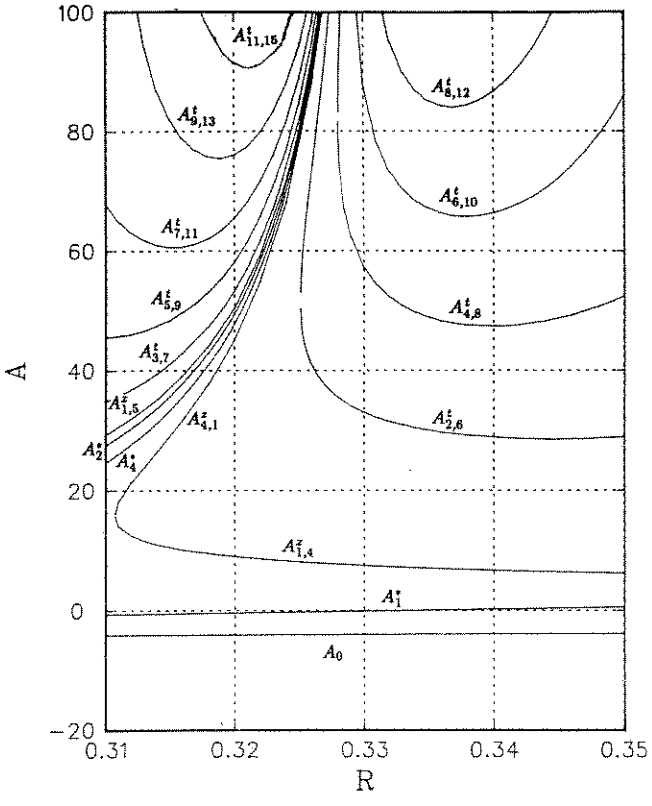

Fig. 3.1. This figure shows the values of A_0 and the various transitions, transferrals, and tangencies for $R \in [0.31, 0.35]$, which affect the geometry of the stability region for $A \leq 100$. Note that some transitions are omitted for clarity.

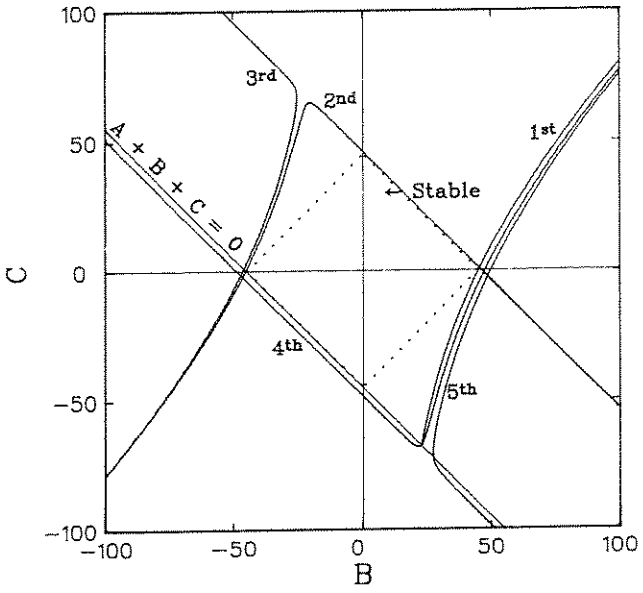

Fig. 3.2. When $R = 0.32$, a reverse transferral occurs at $A^z_{4,1} \simeq 45.0$. This figure shows the first five bifurcation surfaces. Note that the MRS is shown bounded by the dotted lines.

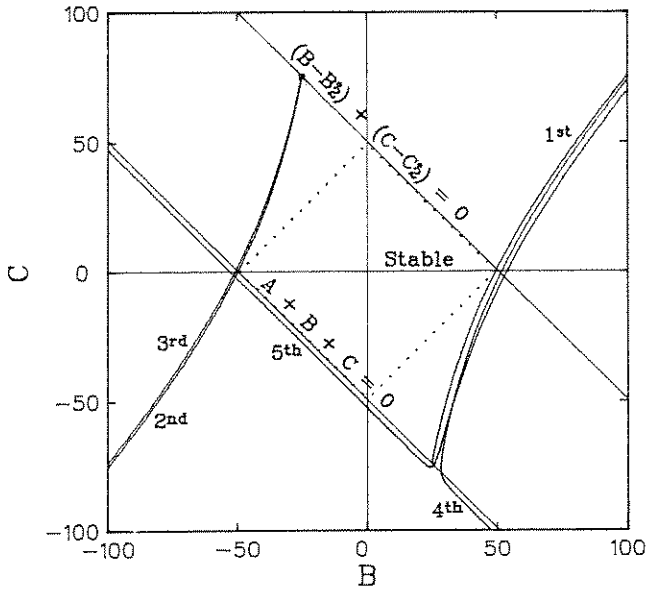

Fig. 3.3. When $R = 0.32$, a transition occurs at $A^*_2 \simeq 49.43$. This figure shows the first five bifurcation surfaces and the line at the transition, $(B - B^*_2) + (C - C^*_2) = 0$.

fourth bifurcation surface to extend out further for its transferral value as it smoothly approaches (2.8). Near $R \simeq 0.311$, A^*_4 has sufficiently stretched the fourth bifurcation surface so that the first transferral does not occur until after A^*_4. For a range of $R < 0.311$, the fifth bifurcation surface becomes the first transferral, $A^z_{1,5}$. Prior to this transferral, there is another change in the stability surface when $R < 0.311$ due to the second transition, A^*_2.

For $R \in (0.311, 0.325)$, the stability surface changes in a manner quite different from the case $R = \frac{1}{3}$. Rather than the next change being the tangency $A^t_{2,6}$, as A increases, the next change in the stability surface is the reverse transferral $A^z_{4,1}$, where the first bifurcation surface displaces the fourth bifurcation surface. (See Fig. 3.2.) In the case $R = 0.32$, the fourth bifurcation surface is incorporated into the stability region boundary at $A^z_{1,4} \simeq 8.86$, then leaves the boundary at $A^z_{4,1} \simeq 45.0$. The geometry of this reverse transferral departs from that in the example of $R = \frac{1}{3}$ presented in Sec. 2 where all curves that join the boundary of the stability region remain part of it.

As A increases further, the second transition, A^*_2, causes the next change in the stability surface and results in the third bifurcation surface becoming part of the boundary. The resulting distortion in the shape of the stability surface is depicted in Fig. 3.3. The transitions A^*_2 and A^*_4 are very close in value for the given range of R. For example, when $R = 0.32$, $A^*_2 \simeq 49.4$ and $A^*_4 \simeq 47.7$. These transitions cause the stability region to extend along the $B + C = \pm A$ lines that bound the MRS and significantly increase the size of the region of stability for a range of A values. All stability surfaces with $R \in [0.31, \frac{1}{3})$ are affected by A^*_2 and have similar distortions. In addition, these transitions have associated stable spurs on the interval (A^p_2, A^*_2) as the third bifurcation curve self-intersects. These stable spurs are much smaller than the ones associated with A^*_1. For example, $A^*_2 - A^p_2 \simeq 4.88 \times 10^{-4}$ at $R = 0.31$ and decreases to $\simeq 2.63 \times 10^{-4}$ when $R = 0.32$. Figure 3.4 shows the next change in the boundary of the stability region as the transferral $A^z_{1,5}$ occurs.

The discussion above shows that for $R < \frac{1}{3}$ even small changes in the delay R may induce a significantly different set of bifurcation surfaces to bound the stability region. Most of these changes result from an even transition or series of even transitions, A^*_{2j}, that cause distortions along the $B + C = \pm A$ lines and do not occur when $R = \frac{1}{3}$. Figure 3.1 can be used to determine which changes occur as R varies. This figure shows that the evolution of the stability surface for $R \in [\frac{1}{3}, 0.35]$ and $A \leq 100$ is much less dramatic.

So how do the odd transitions affect the boundary of the stability region? To examine this issue we consider $R = 0.35$ and $A < 250$. Figure 3.5 shows how A^*_{11}, $A^t_{8,12}$, and $A^t_{8,11}$ vary with R. For $R = 0.35$, a tangency occurs at $A_{8,11} \simeq 144$. As A increases, a transition occurs at $A^*_{11} \simeq 216$, which causes the 11th bifurcation surface to be replaced by the 12th bifurcation surface. This is a smooth transition parallel to the line $B - C = A$ and results in little noticeable change in the geometry of the stability region. Thus, the odd transitions near $R = \frac{1}{3}$ affect which bifurcation surface is on the boundary of the stability region according to our definitions, but have little influence on the geometry of the region or the value of the eigenvalues involved in the Hopf bifurcation. The only effect of the A^*_{11} transition is to swap the 11th and 12th bifurcation surfaces in the boundary of the stability region.

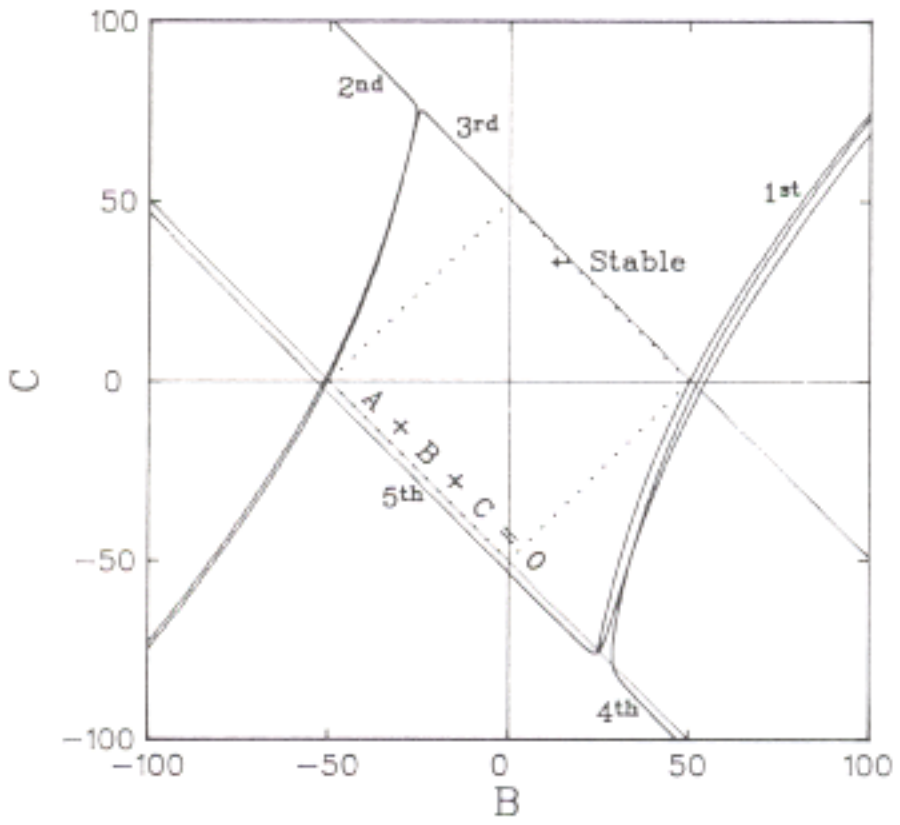

Fig. 3.4. When $R = 0.32$, another transferral occurs at $A^z_{1,5} \simeq 50.4$. This figure shows the first five bifurcation surfaces.

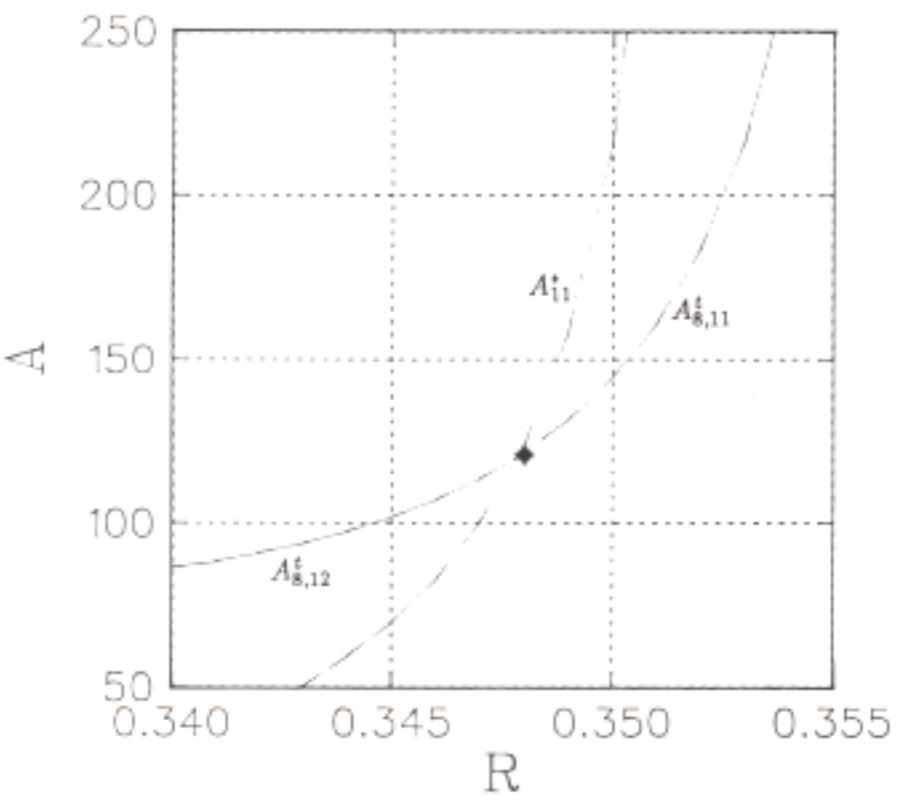

Fig. 3.5. This figure shows the interaction between the transition A^*_{11} and the tangencies $A^t_{8,12}$ and $A^t_{8,11}$ for $R \in [0.34, 0.355]$.

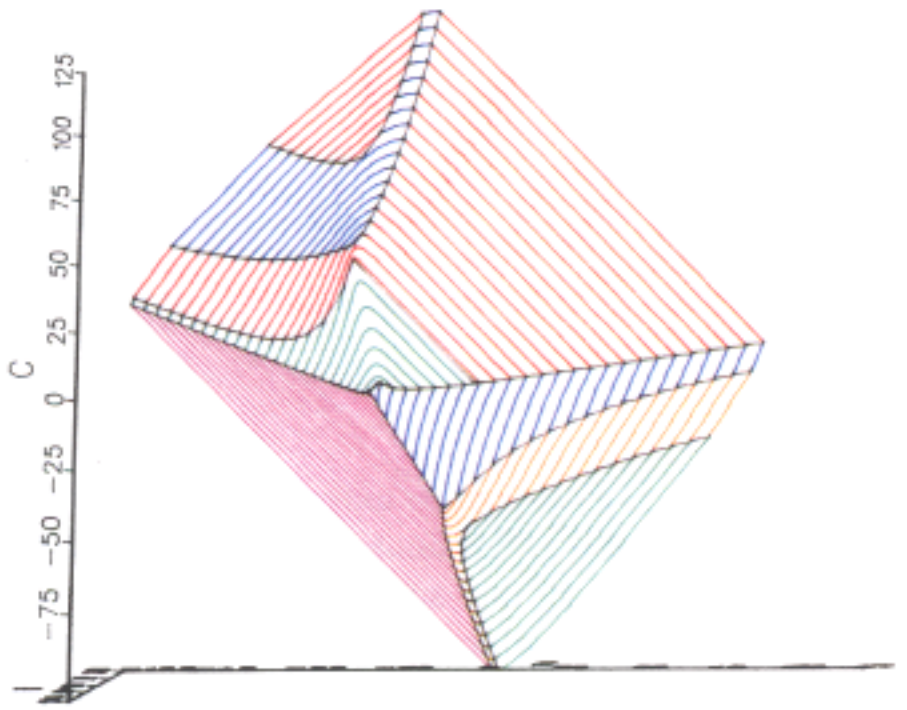

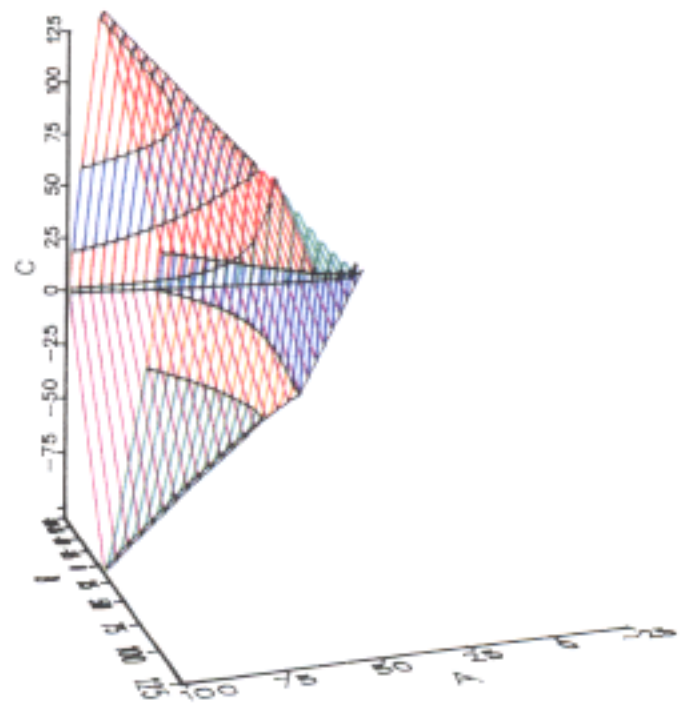

Fig. 3.6. This figure shows two perspectives of the three-dimensional stability surface when $R = 0.31$ and $A \leq 100$. The top view is generated by looking at the stability surface from a point near the A-axis with A large. The bottom view is generated by viewing the stability surface from a point with a large B value.

Figures 3.6–3.10 show the three-dimensional structure of the stability regions for $R = 0.31$, 0.32, $\frac{1}{3}$, 0.34, 0.35 respectively and $A \leq 100$. These graphs are plotted using several colors to emphasize the similarities and differences in their stability regions in the coefficient parameter space.

Comparing the three-dimensional graphs presented in Figs. 3.6–3.10, we note that for reference the $A + B + C = 0$ plane, where a real root crosses the stability surface, is always shown in violet. All of the graphs begin at the point (A_0, B_0, C_0), which exhibits little variation for $R \in [0.31, 0.35]$ and is clearly visible in each of the side perspectives. From this initial point the blue first bifurcation surface rises above the $A + B + C = 0$ plane, then is soon joined by the green second bifurcation surface via the transition A_1^*. The graphs are drawn with a small black line segment at A_1^*, but distortions due to transitions are diminished given the scale of the drawings. Moreover, in order to display a large portion of the stability surface, stable spurs are too small to be visible.

Graphically, the five stability surfaces resemble one another in the early stages in their evolution due to the continuity between delays. However, the three-dimensional graphs clearly show dissimilarities between the cases $R < \frac{1}{3}$ and $R \geq \frac{1}{3}$ for larger

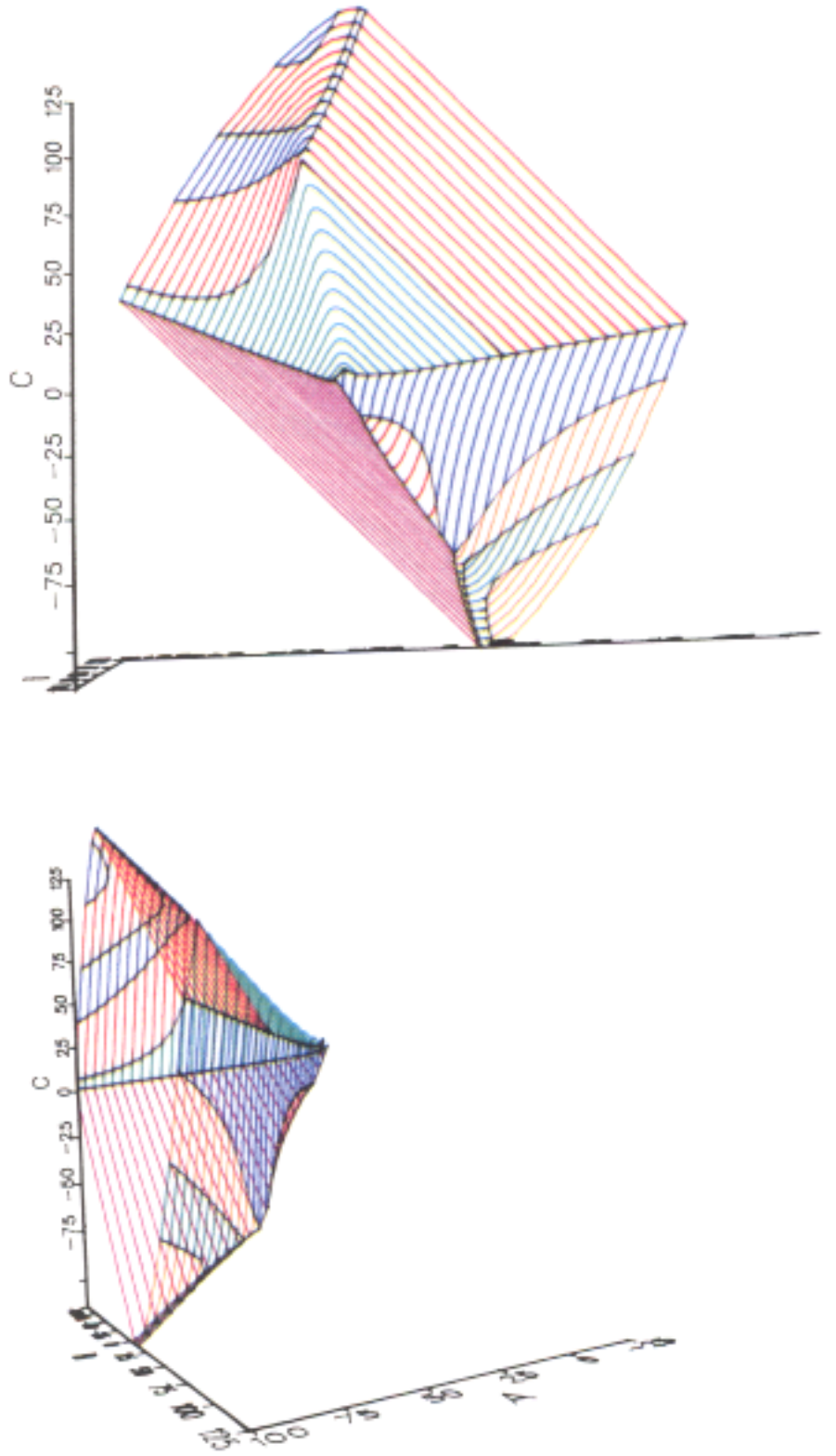

Fig. 3.7. This figure shows two perspectives of the three-dimensional stability surface when $R = 0.32$ and $A \leq 100$. The perspectives are similar to the ones used in Fig. 3.6.

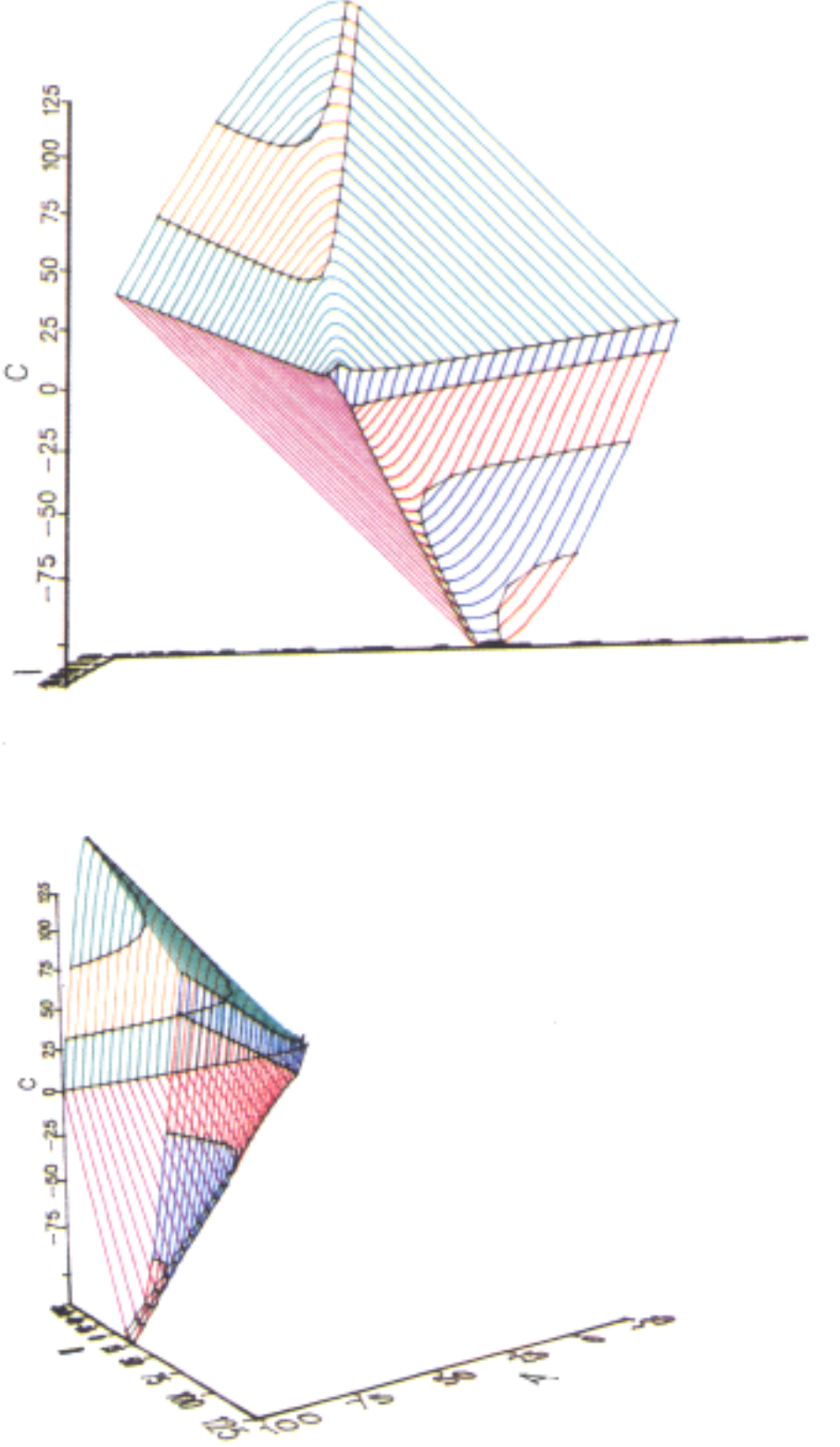

Fig. 3.8. This figure shows two perspectives of the three-dimensional stability surface when $R = \frac{1}{3}$ and $A \leq 100$. The perspectives are similar to the ones used in Fig. 3.6.

values of A, even though some geometric resemblance is maintained. For the sequence of graphs in Figs. 3.8–3.10, the next change in the stability surface following the A_1^* transition is the transferral $A_{1,4}^z$. This transferral appears in the figures as the red 4th bifurcation surface enters the stability surface above the $A + B + C = 0$ plane and encroaches upon the blue first bifurcation surface. After $A_{1,4}^z$, the only changes seen in the stability region for $A \leq 100$ are surfaces appearing through tangencies, which result from higher frequency Hopf bifurcations. Looking at the top graphs in Figs. 3.8–3.10, we see that the sequence of tangencies, $A_{2,6}^t$, $A_{4,8}^t$, $A_{6,10}^t$, and $A_{8,12}^t$ (the last not appearing for $R = 0.35$), alternates with first the orange 6th bifurcation surface appearing in the upper left portion of the stability surface, then the blue 8th bifurcation surface in the lower right portion, then the green 10th bifurcation surface again above and to the left, and finally the red 12th bifurcation surface in the lower right portion of the stability surface.

The sequence of changes as seen by our color coding is the same for Figs. 3.8–3.10, although for $R = 0.35$ it can be seen that by $A = 100$ the stability boundary is nearly a square, indicating its approach to the MRS. In fact, the cross-sectional area at $A = 100$ is only 7.96% larger

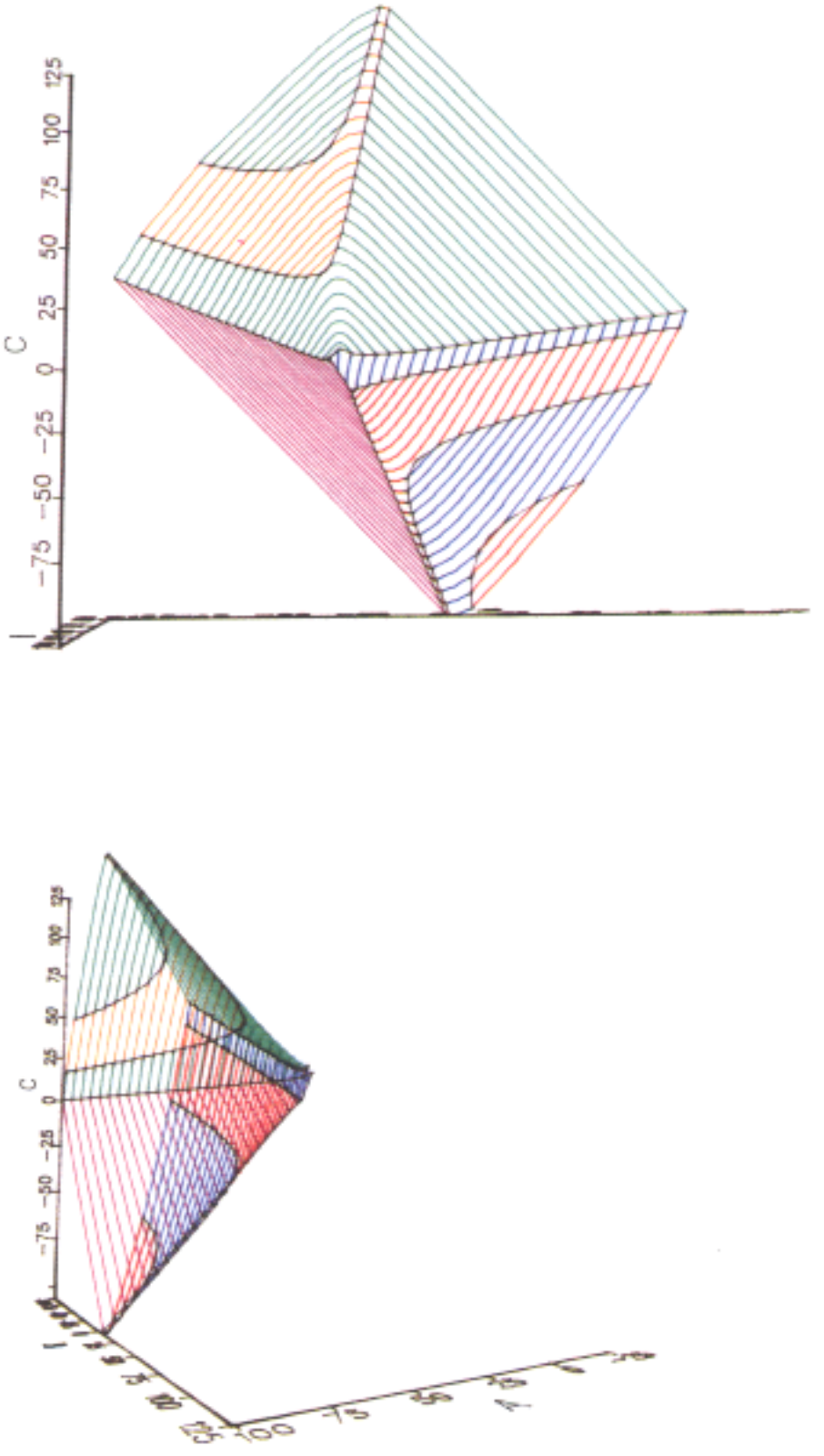

Fig. 3.9. This figure shows two perspectives of the three-dimensional stability surface when $R = 0.34$ and $A \leq 100$. The perspectives are similar to the ones used in Fig. 3.6.

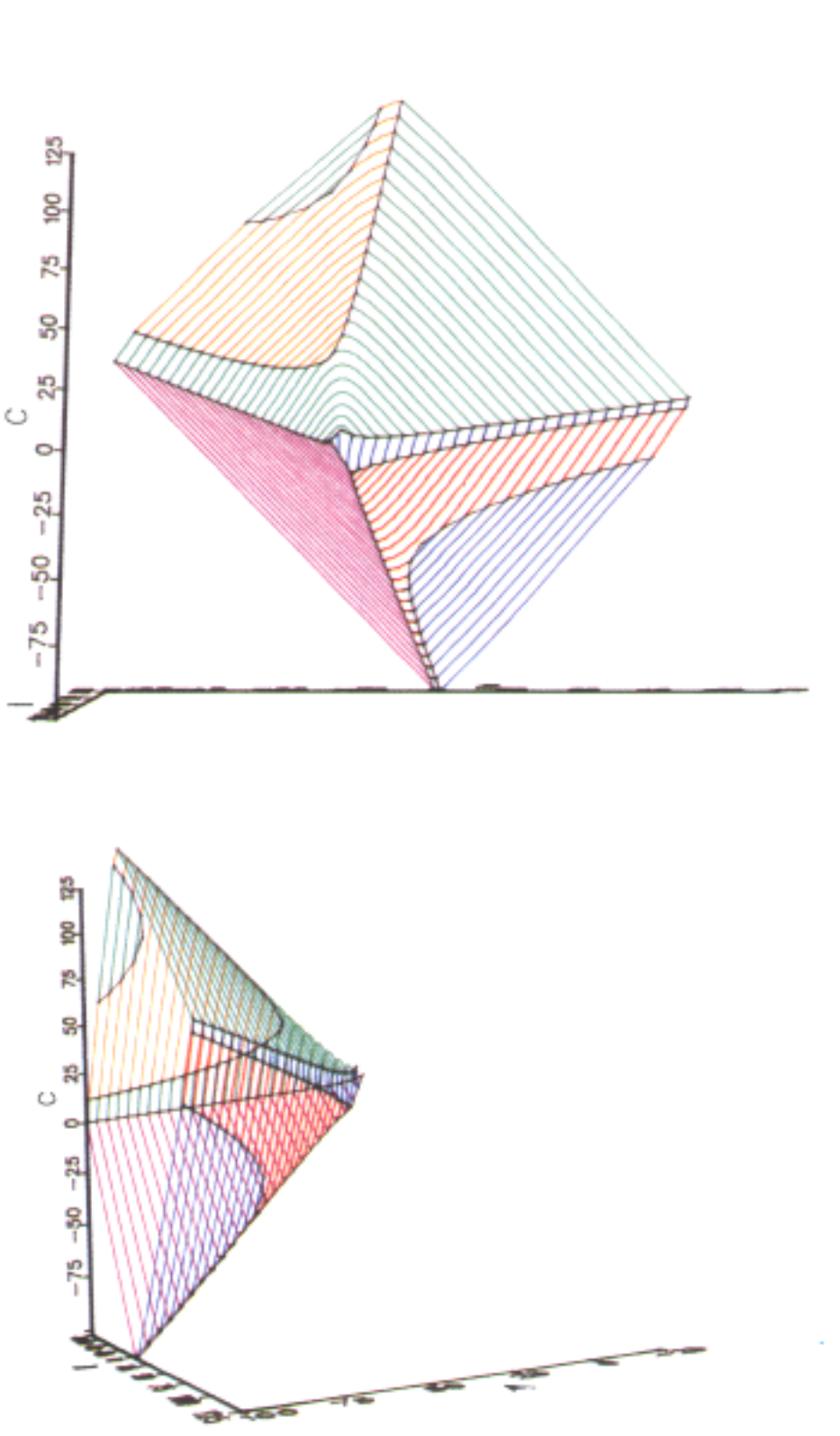

Fig. 3.10. This figure shows two perspectives of the three-dimensional stability surface when $R = 0.35$ and $A \leq 100$. The perspectives are similar to the ones used in Fig. 3.6.

than the MRS for $R = 0.35$, while it is 27.1% larger for $R = \frac{1}{3}$.

For $R < \frac{1}{3}$, the most prominent change in the three-dimensional stability surface is A_2^*, which occurs near $A = 30$ for $R = 0.31$ and near $A = 50$ for $R = 0.32$. In the top graphs for Figs. 3.6 and 3.7, the transition A_2^* is recognizable in the replacement of the green 2nd bifurcation surface with the red 3rd bifurcation surface in the upper right portion of the stability surface. As A increases, the 3rd bifurcation surface expands and displaces more of the 2nd bifurcation surface. For $R = 0.31$ and $R = 0.32$, all of the even transitions occur near A_2^*, which induces a different set of bifurcation surfaces to enter the stability region boundary through transferrals and tangencies as indicated by the variation in the color coding.

A unique feature for $R = 0.32$ among the depicted graphs is the appearance of the red 4th bifurcation surface due to a transferral at $A_{1,4}^z \simeq 8.86$ that terminates in a reverse transferral near $A_{4,1}^z = 45.0$. In both Figs. 3.6 and 3.7, the transition, A_4^*, introduces a new transferral, $A_{1,5}^z$, with the orange 5th bifurcation surface displacing the first bifurcation surface. As noted earlier in this section, the transitions A_2^* and A_4^* cause the stability surface to extend out along the planes $B + C = \pm A$. In the side view graphics of Figs. 3.6 and 3.7, these transitions result in noticeable bulges in the stability surfaces. After the transferral $A_{1,5}^z$, the remainder of the changes in the stability surfaces for $R = 0.31$ and 0.32 and $A \leq 100$ are sequences of tangencies, $A_{3,7}^t$, $A_{5,9}^t$, $A_{7,11}^t$, $A_{9,13}^t$, and $A_{11,15}^t$ (the last two only appear in Fig. 3.7). Again the tangencies appear in an alternating pattern between the upper left and lower right portions of the stability surface in the top figures with different colors indicating which odd-numbered bifurcation surfaces are involved.

Ignoring the color coding which signifies the particular bifurcation surfaces on the boundary of the stability region at $A = 100$, we observe that Fig. 3.6 has more similarities in the shape of its stability region with Fig. 3.10 than any of the other stability surfaces. At $R = 0.31$ and $A = 100$, the stability surface is only 11.1% larger than the MRS. Thus, as R increases or decreases from $R = \frac{1}{3}$ (at least locally), the stability region appears to approach the MRS asymptotically in A. An analysis of the asymptotic behavior of the stability region of (1.3) can be found in Mahaffy *et al.* [1993] and Mahaffy *et al.* [1994].

4. Extensions of the Geometric Analysis for $R \leq \frac{1}{2}$

In the previous section the evolution of the stability surface for (1.3) over a range of R values near $R = \frac{1}{3}$ and A bounded was developed. Herein we extend the analysis of the previous section to delays in the range $0 < R \leq \frac{1}{2}$ for a bounded domain of A. We identify some generic properties of stability surfaces and discuss variations in the construction of the stability region boundary. Extensive numerical studies have established that new bifurcation surfaces enter the boundary of the stability region only through transitions (with associated stable spurs), tangencies, or transferrals as defined in Sec. 2. Figure 4.1 shows the first transition, tangency, and transferral that affect the boundary of the stability region for $R \leq \frac{1}{2}$ and $A \leq 100$.

In Sec. 3, the transition A_1^* for $R \in [0.31, 0.35]$ was shown to be the first change affecting the boundary of the stability region given by Theorem 3.2, which consists of the first bifurcation surface and the $A + B + C = 0$ plane. In fact, we can show numerically that A_1^* is the first change in the stability boundary for all $R_0 < R < 0.47$. Recall that the transition A_1^* has an associated stable spur extending over the range $A \in (A_1^p, A_1^*)$ due to the self-intersection of the second bifurcation surface. Thus, as A increases from A_0 the stability region gains an additional area of stability at $A = A_1^p$, with BC cross-sections showing disjoint stability regions. Numerical studies show that the length of these stable spurs decreases as R increases.

Figure 4.1 shows that A_1^* increases monotonically in R, with asymptotes at $R = 0$ and $R = \frac{1}{2}$. This figure does not include other transitions which may affect the boundary of the stability region. Nevertheless, the influence of these transitions can be surmised from the figure. Even numbered transitions cause the asymptotes in the transferral and tangency curves, partitioning the figure into a set of continuous curves. Each transferral pair, $A_{1,2n}^z$, $A_{1,2n-1}^z$, is circumscribed by even transition asymptotes and is bisected by an odd transition at the point indicated by a diamond. Lying above every adjacent transferral pair are two tangency curves, also bisected by odd transitions at the diamond. As R decreases from $\frac{1}{2}$, the transferral and tangency curves narrow with the minimum of each curve increasing as $R \to 0$. Moreover, higher frequency transitions decrease the gaps between transferral and tangency curves, as can be seen from the

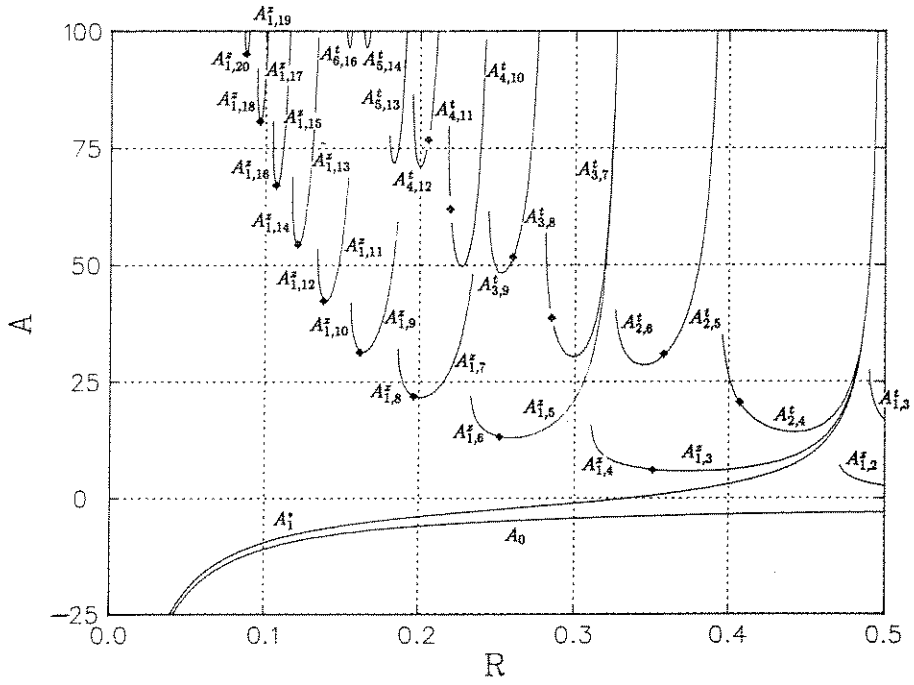

Fig. 4.1. This figure shows the values of A_0, A_1^*, and various transferrals and tangencies for $R \in (0, \frac{1}{2}]$, which affect the geometry of the stability region for $A \leq 100$.

period of the cotangent function in (2.6). When R is small, tangencies and tranferrals do not occur until A becomes large. As a result when R is near zero, an increasing number of transitions affect the boundary of the stability region before any other changes occur.

In order to illustrate the effects that transitions have on the boundary of the stability region as R varies, we examine several examples from $R \in (0, \frac{1}{2}]$. At $R = \frac{1}{2}$, there are no transitions. A transferral occurs at $A_{1,2}^z \simeq 2.61$, after which all other changes to the stability region are the result of tangencies with the first occurring at $A_{1,3}^t \simeq 16.6$. Figure 4.2 shows a BC cross-section at $A = 100$ with the ten bifurcation curves that contribute to the boundary of the stability region. The upper lobe uses only odd curves, while the bottom lobe is constructed from the even bifurcation curves. We note that this stability region is 67.9% larger than the MRS. A more detailed study of the asymptotic behavior appears in Mahaffy *et al.* [1994] and shows that this enlarged stability region remains for $R = \frac{1}{2}$.

For $R \in [\frac{1}{3}, \frac{1}{2})$, there is only one transition that directly affects the boundary of the stability region. On this interval the associated stable spurs are relatively small. As noted in the previous section, it is these transitions that locally create the largest distortions in the stability region.

As R decreases from $\frac{1}{3}$, there are more transitions that affect the construction of the boundary of the stability region. In the case $R = 0.1$ with $A \leq 100$, there are no tangencies though a transferral occurs at $A_{1,17}^z = 91.7$. On the other hand, there are eight transitions, $A_i^* = -9.59, -8.32, -6.05, -2.46, 3.08, 12.09, 29.12, 76.72$, $i = 1, \ldots, 8$, which affect the boundary of the stability region. Each transition causes a new bifurcation surface to enter the boundary of the stability region, increasing its geometric complexity. The stable spurs associated with the transitions, A_i^*, $i = 1, \ldots, 8$, have interval lengths (A_i^p, A_i^*) of 0.688, 0.449, 0.277, 0.156, 0.076, 0.029, 0.007, and 0.001, respectively. Thus, stable spurs are smaller for higher frequency transitions. Unlike the cases previously discussed, the stable spur originating from A_1^* when $R = 0.1$ is relatively large compared to the stability surface emanating from A_0. The length of the interval (A_1^p, A_1^*) is 49% of the length of the interval (A_0, A_1^*), so locally this stable spur represents a significant portion of the stability region. This is shown in Fig. 4.3 for a cross-section at $A = -9.6$. Nevertheless, given the scale of Fig. 4.3, the area of the stable spur relative to the entire stability region is still quite

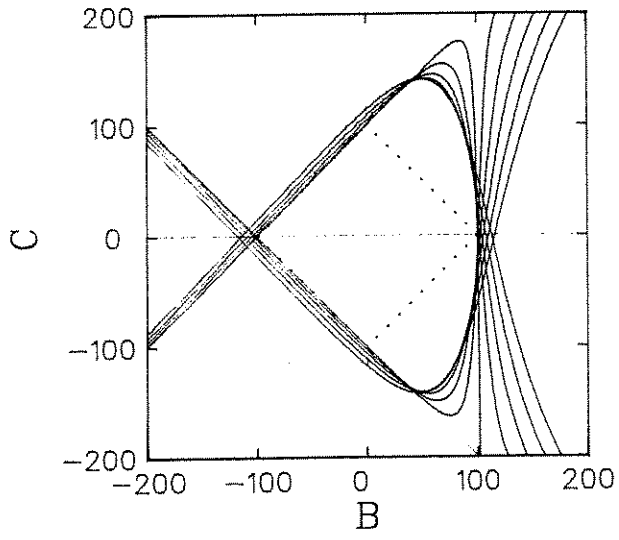

Fig. 4.2. This figure shows a cross-section of the BC-plane at $A = 100$ for $R = 0.5$ with the first 10 bifurcation surfaces bounding the stability region. The dotted lines show the MRS.

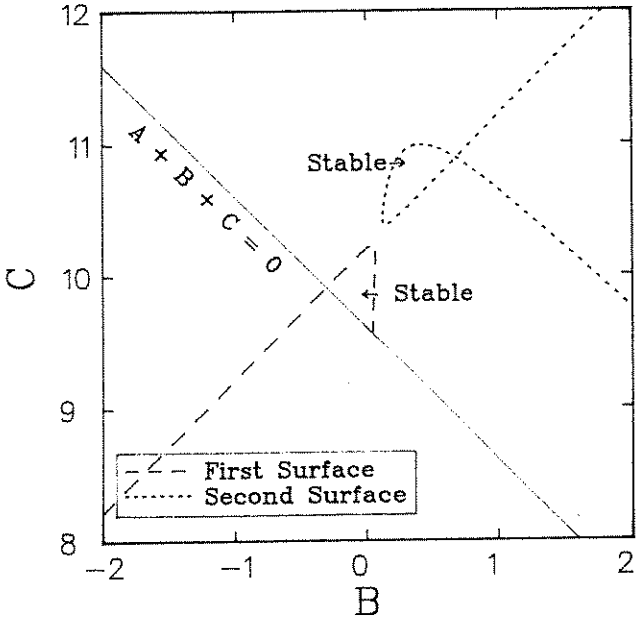

Fig. 4.3. A magnified BC cross-section at $A = -9.6$ when $R = 0.1$ showing that the area of the stable spur can approach the size of the stability region emanating from A_0.

small. An estimate of the total area of stability is approximately $\frac{1}{4}$ square unit.

Transitions, especially the even ones, have the greatest effect on the geometry of the stability region and the eigenvalues that determine stability. However, transferrals and tangencies also contribute to the composition of the stability region. For example, when $0.47 < R < \frac{1}{2}$, the first change in the stability region is a transferral, as seen in Fig. 4.1. As R decreases, the figure shows that the first transferral occurs for increasingly higher bifurcation surfaces due to intervening transitions. For most values of $R \in (0, \frac{1}{2}]$, there is only one transferral that impinges on the boundary of the stability region. This figure does not illustrate the reverse transferrals which occur as a result of even transitions distorting a bifurcation surface along the $A+B+C = 0$ plane, but these would appear in the figure at the jump between $A^z_{1,2n}$ and $A^z_{1,2n+1}$ due to A^*_{2n} as R decreases. In Sec. 3, this situation was described in detail for $R = 0.32$ with Figs. 3.2–3.4 depicting changes in the geometry of the stability region.

The markers on the transferral curves in Fig. 4.1 indicate odd transitions, which determine the particular bifurcation surface involved in a transferral. The figure shows that the change in A with respect to R is continuous for odd transitions along these transferrals. As a result, the geometric appearance of the stability region is maintained as A passes through an odd transition. For example, when $R = 0.351$, A^*_3 causes the fourth bifurcation surface to replace the first bifurcation surface as one of the surfaces intersecting the $A + B + C = 0$ plane, while at $R = 0.352$, it is the third bifurcation surface which enters the boundary of the stability region. However, $A^z_{1,4} \simeq 6.09$ at $R = 0.351$, and $A^z_{1,3} \simeq 6.00$ at $R = 0.352$, showing little change in the A value.

A pattern can also be discerned from Fig. 4.1 for the tangencies. The figure shows two curves lying above each transferral curve which mimic its shape. Thus, the first tangency always occurs after the first transferral. As noted in Sec. 3, there are cases near even transitions where a surface enters and leaves via a tangency and then reappears on a higher frequency bifurcation surface, often with distortions in the shape of the stability region. Like transferrals, odd transitions result in a change in the number of the bifurcation surfaces involved in a tangency, but the change in A, where the tangency occurs, is continuous in R. Unlike transferrals, after the appearance of the first tangency, many more follow. As R approaches $\frac{1}{2}$, tangencies play an increasingly important role in shaping the boundary of the stability region for a given bounded A.

The analysis of this section shows that there is no predictable pattern in the evolution of the stability surface for $R \in (0, \frac{1}{2}]$. However, by following

transitions, transferrals, and tangencies, we have discovered some guiding principles using numerical schemes for determining the region of stability for any delay $R \leq \frac{1}{2}$.

5. Discussion

Our work has outlined a methodology for identifying and characterizing the stability region in the coefficient parameter space of the two-delay differential equation given by (1.3) when the ratio of delays $R \leq \frac{1}{2}$. For most delays, the stability region begins at a specific point given by Theorem 3.2, which is easily seen in the three-dimensional figures, and is bounded by part of the first bifurcation surface and the $A+B+C=0$ plane. Along the former a Hopf bifurcation occurs, while the latter causes a loss of stability as a real root crosses the imaginary axis in the eigenspace. Increasing the coefficient of the undelayed term, A, we discovered only a limited number of ways in which changes to the boundary of the stability region occur.

The most significant changes resulted from transitions, denoted by A_j^*. If the jth bifurcation surface is part of the boundary of the stability region when $A < A_j^*$, at A_j^* a degeneracy occurs as two bifurcation curves meet at a point inducing a Hopf bifurcation with eigenvalues $\lambda = \pm i \frac{j\pi}{1-R}$ along part of the line given by (2.8). At the transition, a stable spur from the self-intersection of the $(j+1)$st bifurcation surface joins the stability region. Subsequently, the $(j+1)$st bifurcation surface enters the boundary of the stability region. A major distortion in the boundary of the stability region occurs during a transition as the asymptotic limits of the two bifurcation surfaces involved swap positions.

For $R \leq \frac{1}{2}$, we observed only two other ways in which new bifurcation surfaces could enter the boundary of the stability region, transferrals and tangencies, as defined in Sec. 2. By studying the way bifurcation surfaces enter the boundary of the stability region, we were able to develop numerical methods to trace the evolution of the stability region for a given value of R and bounded values of A. As noted in the introduction, our numerical routines follow transferrals and tangencies when the two-delay differential equation has two purely imaginary pairs of eigenvalues. Along these intersections a nonlinear problem would use the bifurcation analysis from a two-torus, as seen in Guckenheimer & Holmes [1983], which could result in complicated dynamics.

In Sec. 3, we presented a series of three-dimensional plots showing how the stability regions vary with R, often observing significant changes when R is slightly perturbed. In Sec. 4, this methodology for characterizing the stability region of a linear differential equation with two delays was extended to the interval $(0, \frac{1}{2}]$. In doing so, we demonstrated the significance of transitions and their associated stable spurs as R decreases within the stated interval. Our analysis shows that the shape and size of the stability region is very sensitive to changes in the parameters, especially R.

This paper provides an algorithmic approach to determining the stability of (1.3). Our analysis has revealed the complex nature of the stability surface, yet has not addressed several important issues. We limited this study to the range of $R \leq \frac{1}{2}$ since the bifurcation curves are then simpler. Over this range the bifurcation curves rarely self-intersect, which is not the case when $R > \frac{1}{2}$. We have noted that transitions create the most significant changes in the region of stability and observed that as $R \to 0$ transitions occur more frequently with larger stable spurs. More studies are needed for small values of R. In addition, the asymptotic behavior of stability regions has not been examined. Elsewhere [Mahaffy *et al.*, 1993, 1994] we have shown that for particular values of R the asymptotic region of stability approaches the Minimum Region of Stability, while for other ratios of the delays the stability region always remains larger than the MRS.

Clearly the characterization of the stability region for a two-delay differential equation is a formidible task. We view the results contained herein as a framework within which applications utilizing differential equations with two delays can be studied.

Acknowledgments

The work of Joseph Mahaffy was supported in part by NSF grants DMS-8807360, DMS-9007718, and DMS-9208290. Paul Zak was partially supported under the REU program of NSF by grant DMS-8807360 and by the University of Pennsylvania, and is currently in the Department of Economics at the Claremont Graduate School, Claremont, CA. Kathyrn Joiner was supported by the REU program of NSF by grant DMS-9007718 and currently resides in Bothell, WA.

The ideas of this paper were first presented at a conference at the Claremont Colleges in honor

of Kenneth Cooke in January 1990. The long delay in producing this paper is due to the geometric nature of the project and the complicated nature of differential equations with two delays.

References

Bélair, J. [1987] "Stability of a differential-delay equation with two time delays," in *Oscillations, Bifurcations, and Chaos*, eds. Atkinson, F. V., Langford, W. F. & Mingarelli, A. B. (AMS) pp. 305–315.

Bélair, J. & Campbell, S. A. [1994] "Stability and bifurcations of equilibria in a multiple-delayed differential equation," *SIAM J. Appl. Math.*, in press.

Bélair, J. & Mackey, M. [1987] "A model for the regulation of mammalian platelet production," *Ann. N. Y. Acad. Sci.* **1**, 1–3.

Bélair, J. & Mackey, M. [1989] "Consumer memory and price fluctuations in commodity markets: An integrodifferential model," *J. Dyn. and Diff. Eqns.* **3**, 299–325.

Bélair, J., Mackey, M. & Mahaffy, J. M. [1994] "Age-structured and two delay models for erythropoiesis," *Math. Biosci.*, in press.

Beuter, A., Bélair, J. & Labrie, C. [1993] "Feedback and delays in neurological diseases: A modeling study using dynamical systems," *Bull. Math. Biol.* **55**, 525–541.

Boese, F. G. [1993] "The delay-independent stability behaviour of a first order differential-difference equation with two constant lags," preprint.

Braddock, R. D. & van den Driessche, P. [1981] "A population model with two time delays," in *Quantitative Population Dynamics*, eds. Chapman, D. G. & Gallucci, V. F. (International Cooperative Publishing House, Fairland, MD).

Braddock, R. D. & van den Driessche, P. [1983] "On a two lag differential delay equation," *J. Austral. Math. Soc.* **24**, 292–317.

Busenberg, S. N. & Cooke, K. L. [1984] "Stability conditions for linear non-autonomous delay differential equations," *Quart. Appl. Math.* **42**, 295–306.

Campbell, S. A. & Bélair, J. [1993] "Delays and tori in a nonlinear model from motor control," in *Chaos in Biology and Medicine*, ed. Ditto, W., SPIE Proceedings Series Vol. 2036, pp. 256–268.

Cooke, K. L. & Ferreira, J. M. [1983] "Stability conditions for linear retarded functional differential equations," *J. Math. Anal. Appl.* **96**, 480–504.

Cooke, K. & van den Driessche, P. [1986] "On zeroes of some transcendental equations," *Funckcialaj Ekvacioj* **29**, 77–90.

Cooke, K. L. & Yorke, J. A. [1973] "Some equations modelling growth processes and gonorrhea epidemics," *Math. Biosci.* **16**, 75–101.

El'sgol'ts, L. E. (translated by R. J. McLaughlin) [1966] *Introduction to the Theory of Differential Equations with Deviating Arguments* (Holden-Day, Inc., San Francisco).

Guckheimer, J. & Holmes, P. [1983] *Nonlinear Oscillations, Dynamical Systems, and Bifurcation of Vector Fields* (Springer-Verlag, New York).

Hale, J., Infante, E. & Tsen, P. [1985] "Stability in linear delay equations," *J. Math. Anal. Appl.* **105**, 533–555.

Hale, J. K. [1977] *Theory of Functional Differential Equations* (Springer-Verlag, New York).

Hale, J. K. [1979] *Nonlinear Oscillations in Equations with Delays*, Lectures in Applied Mathematics, Vol. 17 (American Math. Soc., Providence, R. I.).

Hale, J. K. & Huang, W. [1993] "Global geometry of the stable regions for two delay differential equations," *J. Math. Anal. Appl.* **178**, 344–362.

Haller, G. & Stépán, G. [1991] "Codimension two bifurcation in an approximate model for delayed robot control," in *Bifurcation and Chaos: Analysis, Algorithms, Applications*, eds. Seydel, R., Schneider, F. W., Kupper, T. & Troger, H. (Birkhauser, Basel) pp. 155–159.

Hayes, N. [1950] "Roots of the transcendental equation associated with a certain differential difference equation," *J. London Math. Soc.* **25**, 226–232.

Howroyd, T. D. & Russell, A. M. [1984] "Cournot oligopoly models with time lags," *J. Math. Econ.* **13**, 97–103.

Kirk, J., Orr, J. S. & Forrest, J. [1970] "The role of chalone in the control of the bone marrow stem cell population," *Math. Biosc.* **6**, 129–143.

MacDonald, N. [1979] "Cyclical neutropenia; models with two cell types and two time lags," in *Biomathematics and Cell Kinetics*, eds. Valleron, A. J. & Macdonald, P. D. M. (North Holland, Amsterdam), pp. 287–295.

MacDonald, N. [1980] "An activation-inhibition model of cyclic granulopoiesis in chronic granulocytic leukemia," *Math. Biosci.* **54**, 61–70.

MacDonald, N. [1986] "Two delays may not destabilise although either delay can," *Math. Biosci.* **82**, 127–140.

MacDonald, N. [1989] *Biological Delay Systems: Linear Stability Theory* (Cambridge University Press, New York).

Mackey, M. C. [1989] "Commodity price fluctuations: Price dependent delays and nonlinearities as explanatory factors," *J. Econ. Theory* **48**, 497–509.

Mahaffy, J. M., Zak, P. J. & Joiner, K. M. [1993] *A Three Parameter Stability Analysis for a Linear Differential Equation with Two Delays*, Technical Report (Department of Mathematical Sciences, San Diego State University, San Diego, CA).

Mahaffy, J. M., Zak, P. J. & Joiner, K. M. [1994] "Some asymptotic properties of a linear differential equation with two delays," in preparation.

Marriott, C., Valleé, R. & Delisle, C. [1989] "Analysis of a first order differential-delay equation containing two delays," *Phys. Rev.* **A40**, 3420–3428.

Mizuno, M. & Ikeda, K. [1989] "An unstable mode selection rule: Frustrated optical instability due to two competing boundary conditions," *Physica* **D36**, 327–342.

Murdoch, W. W., Nisbet, R. M., Blythe, S. P., Gurney, W. S. C. & Reeve, J. D. [1987] "An invulnerable age class and stability in delay-differential parasitoid-host models," *American Naturalist* **129**, 263–282.

Nussbaum, R. D. [1975] "Differential delay equations with two time lags," *Mem. Amer. Math. Soc.* **16**, 1–62.

Ruiz-Claeyssen, J. [1976] "Effects of delays on functional differential equations," *J. Diff. Eq.* **20**, 404–440.

Silkowski, R. [1979] "A star-shaped condition for stability of linear retarded functional differential equations," *Proc. Roy. Soc. Edinburgh* **A83**, 189–198.

Stépán, G. [1987] *Delay as Bifurcation Parameter*, International Series of Numerical Mathematics, Vol. 79 (Birkhäuser Verlag, Basel).

Zaron, E. [1987] *The Delay Differential Equation:* $x'(t) = -ax(t) + bx(t - \tau_1) + cx(t - \tau_2)$, Technical Report (Harvey Mudd College, Claremont, CA).